How vadose zone mass and energy transfer physics affects the ecohydrological dynamics of a Tibetan meadow?

Lianyu Yu[1], Yijian Zeng[1], Simone Fatichi[2], Zhongbo Su[1,3]

[1] Faculty of Geo-information and Earth Observation (ITC), University of Twente, Enschede, The Netherlands

[2] Department of Civil and Environmental Engineering, National University of Singapore, Singapore

[3] Key Laboratory of Subsurface Hydrology and Ecological Effect in Arid Region of Ministry of Education, School of Water and Environment, Chang'an University, Xi'an, China

Correspondence to: Yijian Zeng (y.zeng@utwente.nl); Zhongbo Su (z.su@utwente.nl)

Abstract. The vadose zone is a sensitive region to environmental changes and exerts a crucial control in ecosystem functioning. While the way in representing the underlying process of vadose zone differs among models, the effect of such differences on ecosystem functioning is seldomly reported. Here, the detailed vadose zone process model STEMMUS was coupled with the ecohydrological model T&C to investigate the role of solving influential physical processes, considering different soil water and heat transfer parameterizations including frozen soils. We tested model performance with the aid of a comprehensive observation dataset collected at a typical meadow ecosystem on the Tibetan Plateau. Results indicated that: i) explicitly considering the frozen soil process significantly improved the soil moisture/temperature (SM/ST) profile simulations and facilitated our understanding of the water transfer processes within the soil-plant-atmosphere continuum; ii) the difference among various complexity of vadose zone physics have an impact on the vegetation dynamics mainly at the beginning of the growing season; iii) models with different vadose zone physics can predict similar interannual vegetation dynamics, and energy, water and carbon exchanges at the land-surface. This research highlights the role of vadose zone models and their underlying physics, in ecosystem functioning and can guide the development and applications of future earth system models.

1. Introduction

Understanding how ecosystem functioning interacts with changing environmental conditions is a crucial yet challenging problem of earth system research. Various types of models, including land surface models, terrestrial biosphere models, ecohydrology models, and hydrological models, have been widely utilized to enhance our knowledge in terms of land surface and hydrological processes including the role of vegetation (Fatichi et al., 2016a;Fisher et al., 2014). A number of uncertainties are originated from different model structures. A more detailed knowledge of the effect of using a given model formulation can help toward making better projections of land surface dynamics, also in response to the call for joint efforts for systematic model developments (Clark et al., 2015;Yu et al., 2016). With emphasis on enhancing the underlying physics, most of the models have already adopted various solutions and parameterizations of land surface processes (e.g., Noah MP, CLM5, T&C) (Fatichi et al., 2012a, b;Niu et al., 2011;Lawrence et al., 2019), which facilitate the appropriate descriptions of different physical processes in various ecosystems. However, in these models, the water and heat transfer process in the vadose zone remains independent and uncoupled, as they often adopt simplified approaches to water and heat transfer in the subsurface. Such physical parameterizations of vadose zone might result in unsatisfactory simulations or physical interpretations, especially when water and heat are tightly coupled as for instance in freezing soils (Hansson et al., 2004). In this regard, researchers have stressed the necessity to simultaneously consider the water and heat transfer process in dry/cold seasons (Bittelli et al., 2008;Scanlon and Milly, 1994;Yu et al., 2016;Yu et al., 2018;Zeng et al., 2009a;Zeng et al., 2009b).

With the largest area of high-altitude permafrost and seasonally frozen ground, Tibetan Plateau is recognized as one of the most sensitive regions for climate change (Cheng and Wu, 2007;Liu and Chen, 2000). Monitoring and projecting the dynamics of hydrothermal and ecohydrological states and their responses to climate change in the Tibetan Plateau is considerably important to help shedding light on future ecosystem responses. Considerable land-surface and vegetation changes have been reported, e.g., degradation of permafrost and changes of frozen ground (Cheng and Wu, 2007), advancing vegetation leaf onset dates (Zhang et al., 2013), and enhanced vegetation activity at start of growing season (Qin et al., 2016). However, there are divergences with regard to the expected ecosystem modifications across the Tibetan Plateau (Qin et al., 2016;Wang et al., 2018;Zhao et al., 2010). It is thus fundamental to have in situ multicomponent measurement networks (including meteorology, soil moisture/temperature, surface energy fluxes, carbon fluxes) to understand the environmental controls (Hao et al., 2011;Wang et al., 2018;Wang et al., 2017;Zhao et al., 2010), validate terrestrial biosphere models and remote sensing products (He et al., 2014;Mwangi et al., 2020;Niu et al., 2016;Su et al., 2013;Tian et al., 2017), and extrapolate results via model-data-fusion methods to larger scales to better characterize land surface processes and ecosystem dynamics of the Tibetan Plateau (He et al., 2014;Zeng et al., 2016;Zhuang et al., 2020).

In this study, we tested the consequences of considering coupled water and heat transfer processes on land-surface fluxes and ecosystem dynamics in the extreme environmental conditions of the Tibetan plateau

relying on state-of-the-art land-surface and ecohydrological modeling confronted with multiple field observations. The limited knowledge of including or not complex vadose zone processes in such environment

70 frames the scope here. Specifically, the driving questions of the research are: i) How different complexity in representing frozen soil and coupled water and heat physics is affecting the simulated ecohydrological dynamics of a Tibetan plateau meadow? ii) How does model complexity affect our interpretation of mass, energy, and carbon fluxes at the ecosystem scale? Answering these questions is important to evaluate the adequacy of models to answer questions related ecosystem changes across the Tibetan Plateau.

75 In order to achieve the aforementioned goals, the detailed soil mass and energy transfer process developed in the STEMMUS model (Zeng et al., 2011a, b;Zeng and Su, 2013) was incorporated into the ecohydrology model Tethys-Chloris (T&C) (Fatichi et al., 2012a, b). The frozen soil physics was explicitly taken into account and soil water and heat transfer are fully coupled to further facilitating the model's capability in dealing with complex vadose zone processes.

2 Methods

2.1 Experimental site

The Maqu soil moisture and soil temperature (SMST) monitoring network (Dente et al., 2012;Su et al., 2011;Su et al., 2013;Zeng et al., 2016) is situated on the north-eastern fringe of the Tibetan Plateau. The monitoring network covers an area of approximately 40 km×80 km (33°30'–34°15'N, 101°38'–102°45'E)

85 with the elevation varying from 3200 m to 4200 m above the sea level (a.s.l.). The climate can be characterized by wet rainy summers and cold dry winters. The mean annual air temperature (MAT) is 1.2°C with about -10.0°C and 11.7°C for the coldest month (January) and warmest month (July), respectively. The alpine meadows (e.g., *Cyperaceae* and *Gramineae*) dominate in this region with the height of about 5 cm during the wintertime and 15 cm during the summertime. The general soil types are categorized as sandy

90 loam, silt loam with a maximum of 18.3 % organic matter for the upper soil layers(Dente et al., 2012;Zhao et al., 2018;Zheng et al., 2015a;Zheng et al., 2015b). The groundwater level of the grassland area fluctuates from about 8.5 m to 12.0 m below the ground.

At Maqu site, SMST profiles (5 cm, 10 cm, 20 cm, 40 cm, and 80 cm) are automatically measured by 5 TM ECH$_2$O probes (METER Group, Inc., USA) at a 15-min interval. The meteorological forcing (including wind

95 speed/direction, air temperature and relative humidity at five heights above ground) is recorded by a 20 m Planetary Boundary Layer (PBL) tower system. An eddy-covariance system (EC150, Campbell Scientific, Inc., USA) was installed for monitoring the dynamics of the turbulent heat fluxes and carbon fluxes. Instrumentations for measuring four component down and upwelling solar and thermal radiation (NR01-L, Campbell Scientific, Inc., USA), and liquid precipitation (T200B, Geoner, Inc., USA) are also deployed. For

100 this research, data from March 2016 to August 2018 collected at the central experimental site (33°54'59"N, 102°09'32", elevation: 3430m) were utilized. We downloaded MCD15A3H (Myneni et al., 2015) and MOD17A2H (Running Steve et al., 2015) products as representative of remotely sensed vegetation dynamics

data from the Oak Ridge National Laboratory Distributed Active Center (ORNL DAAC) website.
MCD15A3H provides estimation of 8-day composites of LAI and FPAR, while MOD17A2H an 8-day

105   composite of Gross Primary Production (*GPP*). Both MODIS products are at a resolution of 500m.

2.2 Land surface carbon fluxes

Starting from the raw *NEE* (Net Ecosystem Exchange) and ancillary meteorological data (friction velocity
u_*, global radiation R_g, soil temperature T_{soil}, air temperature T_{air}, and vapor pressure deficit VPD), we
employed the REddyProc package (Reichstein et al., 2005;Wutzler et al., 2018) as post-processing tool to

110   obtain the time series of *NEE*, *GPP* (Gross Primary Production) and ecosystem respiration R_{eco} dynamics.
Three different techniques, u_* filtering, gap filling, and flux partitioning, were adopted in REddyProc
package. The periods with low turbulent mixing is firstly determined and filtered for quality control
(u_* filtering, (Papale et al., 2006)). Then, the marginal distribution sampling (MDS) algorithm was used as
the gap filling method to replace the missing data (Reichstein et al., 2005). Finally, NEE was separated into

115   GPP and R_{eco} by night-time based and day-time based approaches (Lasslop et al., 2010).

2.3 Precipitation, evapotranspiration, and frost front

The observed surface water conditions over the entire study period, including the precipitation and
cumulative evapotranspiration (which is obtained by summing up the hourly latent heat flux measured by EC
system), are shown in Fig. 1a. Both ET and precipitation are low until the end of the freezing period (see Fig.

120   1b), during this early period the daily average ET is 0.15 mm/d. During the growing season, the cumulative
precipitation increases and ET follows with a lower magnitude. The average daily ET for the entire
observation period is 1.45 mm/d.

Figure 1b presents the development of freezing depth with time (the freezing depth development of year
2017-2018 was incomplete due to the absence of soil temperature data). Several freezing/thawing cycles

125   frequently occurred at the beginning of the winter, which initializes the Freezing-Thawing (FT) process. Frost
front starts to propagate with a rate of 1.34 cm/d, reaching its maximum depth at around 80cm for the year
2016-2017. Then the thawing process is activated by the atmospheric forcing and subsurface soil heat flux,
acting from the soil surface and bottom soil, respectively.

2.4 Modeling the soil-plant-atmosphere continuum

130   #### 2.4.1 Overview of Tethys-Chloris

The Tethys-Chloris model (T&C) (Fatichi et al., 2012a) simulates the coupled dynamics of energy, water,
and vegetation and has been successfully applied to a very large spectrum of ecosystems and environmental
conditions as summarized elsewhere (Fatichi and Ivanov, 2014;Fatichi and Pappas, 2017;Fatichi et al.,
2016b;Mastrotheodoros et al., 2017;Pappas et al., 2016). The model simulates the energy, water, and carbon

135   exchanges between the land surface and the atmospheric surface layer accounting for aerodynamic,

undercanopy, and leaf boundary layer resistances, as well as for stomatal and soil resistance. The model further describes vegetation physiological processes including photosynthesis, phenology, carbon allocation, and tissue turnover. Dynamics of water content in the soil profile are solved using the one-dimensional (1-D) Richards equation. Heat transfer in the soil is solved by means of the heat diffusion equation. Soil heat

140   and water dynamics are uncoupled. A detailed model description is provided in the above-mentioned references and some key elements for this article are discussed in the following.

2.4.2 Overview of STEMMUS

STEMMUS (**S**imultaneous **T**ransfer of **E**nergy, **M**ass and **M**omentum in **U**nsaturated **S**oil) model solves soil water movement, soil air flow, and soil heat flow balance equations simultaneously in one timestep (Zeng et

145   al. 2011a,b;Zeng and Su, 2013). The Richards' equation with modifications made by Milly (1982) was utilized to mimic the coupled soil mass and energy transfer process. The dry air is considered to be an independent phase in the soil. The vapor diffusion, advection and dispersion are all taken into account as the water vapor transport mechanism. In addition to the soil moisture and temperature gradient, the atmospheric pressure gradient acts as the third driving force for soil water, vapor and heat flow. Root water uptake process

150   is regarded as the sink term of soil water and heat balance equations, building up the linkage between soil and atmosphere (Yu et al., 2016).

2.4.3 Difference between STEMMUS and T&C models in mass and energy transfer process

While T&C model specializes in dealing with the interaction between vegetation and the hydrological system, it simplified the soil water and heat transfer process in the hydrology component, e.g., ignored water vapor

155   flow, dry air flow, and, in the original version, does not contain freezing/thawing process, as water is always in liquid phase regardless of sub-zero soil temperatures. To extend the application of T&C model over frozen soil, a freeze-thaw module has been incorporated for this study as described below. Furthermore, while STEMMUS model can well reproduce the soil water and heat transfer process, it lacks detailed description of land-surface processes and of the vegetation-hydrology feedback mechanisms. To take advantage of the

160   strengths of both models, we coupled STEMMUS with the land-surface and vegetation components of T&C model to better describe the soil-plant-atmosphere continuum.

1) Mass transfer process

The 1-D Richards equation, which describes the water flow under gravity and capillary forces in isothermal conditions, is solved in T&C for variably saturated soils.

$$\frac{\partial \theta}{\partial t} = -\frac{\partial q}{\partial z} - S = \rho_L \frac{\partial}{\partial z}\left[K\left(\frac{\partial \psi}{\partial z} + 1\right)\right] - S \qquad (1)$$

165   where θ (m^3 m^{-3}) is the volumetric water content; q (kg m^{-2} s^{-1}) is the water flux; z (m) is the vertical direction coordinate; S (s^{-1}) is the sink term for transpiration, evaporation and lateral transfer fluxes. ρ_L (kg m^{-3}) is the liquid water density; K (m s^{-1}) is the soil hydraulic conductivity; ψ (m) is the soil water potential; t (s) is the time.

In T&C, the nonlinear partial differential equation is solved using a finite volume approach with the method
of lines (MOL) (Lee et al., 2004). MOL discretizes the spatial domain and reduces the partial differential
equation to a series of ordinary differential equations in terms of time, which can be expressed as

$$d_{z,i}\frac{d\theta_i}{dt} = q_{i-1} - q_i - \left(\sum_{j=1}^{n_c} T_{H_v,j} r_{H_v,i,j}\right) - \left(\sum_{j=1}^{n_c} T_{L_v,j} r_{L_v,i,j}\right) - \left(\sum_{j=1}^{n_c} E_{s,j}\right) - E_{bare} + Q_{l,in,i} \\ - Q_{l,out,i}$$

(2)

where q_i (m s^{-1}) is the vertical outflow from a layer i, T_{Hv} , and T_{Lv} (m s^{-1}) are the transpiration fluxes from
the high- and low-vegetation layers, respectively. E_{bare} (m s^{-1}), evaporation from the bare soil. E_s (m s^{-1}),
evaporation from soil under the canopy. $Q_{l,in,i}$, $Q_{l,out,i}$ (m s^{-1}) are the incoming lateral subsurface fluxes
and lateral outflows, respectively.

While in STEMMUS, temporal dynamics of three phases of water (liquid, vapor and ice), together with the
soil dry air component, are explicitly presented and simultaneously solved by spatially discretizing the
corresponding governing equations of liquid water flow, vapor flow and dry air flow.

$$\frac{\partial}{\partial t}(\rho_L\theta_L + \rho_V\theta_V + \rho_i\theta_{ice}) = -\frac{\partial}{\partial z}(q_{Lh} + q_{LT} + q_{La} + q_{Vh} + q_{VT} + q_{Va}) - S$$
$$= \rho_L\frac{\partial}{\partial z}\left[K\left(\frac{\partial\psi}{\partial z}+1\right) + D_{TD}\frac{\partial T}{\partial z} + \frac{K}{\gamma_w}\frac{\partial P_g}{\partial z}\right] + \frac{\partial}{\partial z}\left[D_{Vh}\frac{\partial\psi}{\partial z} + D_{VT}\frac{\partial T}{\partial z} + D_{Va}\frac{\partial P_g}{\partial z}\right] - S$$

(3)

where ρ_v and ρ_i (kg m^{-3}) are the density of water vapor and ice, respectively; θ_L, θ_V and θ_{ice} (m^3 m^{-3}) are the
soil liquid, vapor and ice volumetric water content, respectively; q_{Lh}, q_{LT}, and q_{La} (kg m^{-2} s^{-1}) are the soil
liquid water flow driven by the gradient of soil matric potential $\frac{\partial\psi}{\partial z}$, temperature $\frac{\partial T}{\partial z}$, and air pressure $\frac{\partial P_g}{\partial z}$,
respectively. q_{Vh}, q_{VT}, and q_{Va} (kg m^{-2} s^{-1}) are the soil water vapor fluxes driven by the gradient of soil matric
potential $\frac{\partial\psi}{\partial z}$, temperature $\frac{\partial T}{\partial z}$, and air pressure $\frac{\partial P_g}{\partial z}$, respectively. T (°C) is the soil temperature; and P_g (Pa) is
the mixed pore-air pressure. γ_W (kg m^{-2} s^{-2}) is the specific weight of water. D_{TD} (kg m^{-1} s^{-1} °C^{-1}) is the
transport coefficient of the adsorbed liquid flow due to temperature gradient; D_{Vh} (kg m^{-2} s^{-1}) is the isothermal
vapor conductivity; and D_{VT} (kg m^{-1} s^{-1} °C^{-1}) is the thermal vapor diffusion coefficient; D_{Va} is the advective
vapor transfer coefficient.

2) Energy transfer process

The heat conservation equation used in the original T&C neglects the coupling of water and heat transfer
physics and only the heat conduction component is considered, which can be expressed as below

$$C_{soil}\frac{\partial T}{\partial t} = \frac{\partial}{\partial z}\left(\lambda_{eff}\frac{\partial T}{\partial z}\right)$$

(4)

where C_{soil} (J kg^{-1} °C^{-1}) is the specific heat capacities of bulk soil; λ_{eff} (W m^{-1} °C^{-1}) is the effective thermal
conductivity of the soil. When soil undergoes freezing/thawing process, the latent heat due to water phase
change becomes important but is not included in the original T&C model.

STEMMUS takes into account different heat transfer mechanisms, including heat conduction ($\lambda_{eff}\frac{\partial T}{\partial z}$),
convective heat transferred by liquid, vapor and air flow, the latent heat of vaporization ($\rho_V\theta_V L_0$), the latent

heat of freezing/thawing $(-\rho_i\theta_i L_f)$ and a source term associated with the exothermic process of wetting of a porous medium (integral heat of wetting) $(-\rho_L W \frac{\partial\theta_L}{\partial t})$.

$$\frac{\partial}{\partial t}\left[(\rho_s\theta_s C_s + \rho_L\theta_L C_L + \rho_V\theta_V C_V + \rho_{da}\theta_a C_a + \rho_i\theta_i C_i)(T - T_r) + \rho_V\theta_V L_0 - \rho_i\theta_i L_f\right] - \rho_L W \frac{\partial\theta_L}{\partial t}$$
$$= \frac{\partial}{\partial z}\left(\lambda_{eff}\frac{\partial T}{\partial z}\right) - \frac{\partial}{\partial z}[q_L C_L(T - T_r) + q_V(L_0 + C_V(T - T_r)) + q_a C_a(T - T_r)] - C_L S(T - T_r) \tag{5}$$

where ρ_s (kg m^{-3}) is the soil solids density; θ_s is the volumetric fraction of solids in the soil; C_s, C_L, C_V, C_a and C_i (J kg^{-1} °C^{-1}) are the specific heat capacities of soil solids, liquid, water vapor, dry air and ice,

200   respectively; T_r (°C) is the arbitrary reference temperature; L_0 (J kg^{-1}) is the latent heat of vaporization of water at the reference temperature; L_f (J kg^{-1}) is the latent heat of fusion; W (J kg^{-1}) is the differential heat of wetting (expressed by Edlefsen and Anderson (1943) as the amount of heat released when a small amount of free water is added to the soil matrix). q_L, q_V, and q_a (kg m^{-2} s^{-1}) are the liquid, vapor water flux and air flow,

205   respectively. Additional details and the air flow balance equation for solving the coupled water and heat equations can be found in Zeng et al. (2011a, b) and Zeng and Su (2013).

2.4.4 T&C model with freezing/thawing process

In the T&C version modified to explicitly account for freezing/thawing processes, the heat conservation equation is written as:

$$C_{soil}\frac{\partial T}{\partial t} - \rho_i L_f \frac{\partial\theta_i}{\partial t} = \frac{\partial}{\partial z}\left(\lambda_{eff}\frac{\partial T}{\partial z}\right) \tag{6}$$

where the latent heat associated with the freezing/thawing process is explicitly considered and ice water

210   content θ_i is a prognostic variable, which is simulated along with liquid water content for each soil layer. Specifically, when Eq. (7) is rewritten in terms of an apparent specific heat capacity C_{app} (Gouttevin et al., 2012;Hansson et al., 2004) it can be solved equivalently to Eq. (4):

$$C_{app}\frac{\partial T}{\partial t} = \frac{\partial}{\partial z}\left(\lambda_{eff}\frac{\partial T}{\partial z}\right) \tag{7}$$

where C_{app} can be computed knowing the temperature T, latent heat of fusion L_f and the differential (specific) water capacity dθ/dψ at a given water content (Hansson et al., 2004):

$$C_{app} = C_{soil} + \rho_i \frac{L_f^2}{gT}\frac{d\theta}{d\psi} \tag{8}$$

215   The effective thermal conductivity λ_{eff} (W m^{-1} °C^{-1}) and the specific soil heat capacity C_{soil} (J kg^{-1} °C^{-1}) are computed accounting for solid particles, water, and ice content (Farouki, 1981;Johansen, 1975;Yu et al., 2018;Lawrence et al., 2018). The soil freezing characteristic curve providing the maximum liquid water content at a given temperature is computed following Dall'Amico et al. (2011) and it can be combined with various soil hydraulic parameterization including van-Genuchten, Clapp and Hornberger and Saxton and

220   Rawls (Fuchs et al., 1978;Yu et al., 2018).

Finally, saturated hydraulic conductivity is corrected in presence of ice content (e.g., (Hansson et al., 2004; Yu et al., 2018)). Note, that beyond latent heat associated with phase change and changes in thermal and hydraulic parameters because of ice presence, all the other soil physics processes described by STEMMUS are neglected and heat and water fluxes are still uncoupled in this version of T&C.

2.5 Coupling procedure

The current coupling procedure between STEMMUS and the original T&C is based on a sequential coupling via exchanging mutual information within one timestep (see Figure 2). T&C model and STEMMUS model ran sequentially within one timestep. First, the preparation and initialization module are called. Meteorology inputs and constant parameters are set, and the initialization process is performed. After the input are prepared, the main iteration process starts. T&C is in charge of the time control information (starting time, time step, elapsed time) and informs STEMMUS model with these time settings every time step. Meanwhile, the surface boundary conditions obtained by the solution of vegetation and land-surface energy dynamics are also sent to drive STEMMUS model. The surface latent heat flux (LE) is partitioned into soil evaporation (used for setting the surface boundary condition of soil water flow) and plant transpiration (further subdivided into layer specific root water uptakes representing the sink terms of Richard equation). After convergence achieves in the soil module, STEMMUS estimates soil temperature/soil moisture (hereafter as ST/SM) profiles, which are utilized to update ST/SM states in T&C model. T&C model then utilizes these updated ST/SM information (rather than its own computed ST/SM profiles) to proceed with the ecohydrological simulations in the following time step. Such iteration continues till the end of simulation period.

2.6 Design of numerical experiment

To investigate the role of increasing complexity of vadose zone physics in ecosystem functioning, three numerical experiments were designed on the basis of aforementioned modeling framework. First experiment, the T&C original model was ran as stand-alone, termed as unCPLD simulation. Second experiment, the updated T&C model with explicit consideration of freezing/thawing process is run as it can estimate the dynamics of soil ice content and the related effect on water and heat transfer (e.g., blocking effect on water flow, heat release/gain due to phase change) but otherwise being exactly equal to T&C original model. This second simulation is named the unCPLD-FT simulation. Third experiment, STEMMUS model was coupled with T&C model to enable one to consider not only a simplified frozen soil physics but also additional processes and most important water and heat effects are tightly coupled and affect each other. This simulation is named CPLD simulation.

All three numerical experiments shared the same soil and vegetation parameter settings to accommodate the conditions of a Tibetan meadow. The total depth of soil column was set as 3m and divided into 18 layers with a finer discretization in the upper soil layers (1-5cm) than that in the lower soil layers (10-50cm). Soil samples were collected and transported to the laboratory to determine the soil hydrothermal properties (see Zhao et al. (2018) for detail). The average soil texture and fitted Van Genuchten parameters at three soil

layers were listed in supplement Table S1. Vegetation parameters were obtained on the basis of physical constraints, literature, and expert knowledge (see a summary of the adopted vegetation parameters in the supplement Table S2).

3 Results

3.1 Surface fluxes simulations

260

The 5-day moving average dynamics of the net incoming radiation (Rn), latent heat (LE) and sensible heat (H) fluxes measured and simulated by the unCPLD model, unCPLD-FT and CPLD model for the study period are presented (Figure 3). The seasonality and magnitude of surface fluxes can be captured across seasons. A good match between observed and simulated Rn and LE was identified during the whole period,

265 with isolated observable discrepancies (Fig. 3a &c). These mismatches of Rn can be partly attributed to the uncertainties of observed winter precipitation events and the following snow cover dynamics, which might not be well captured in the models, because the true winter precipitation is difficult to observe. For the sensible heat flux simulations, all three models can reproduce the seasonal dynamics. However, an overestimation of the 5-day average values was observed in several periods. Given the good correspondence

270 between observations and simulations of net radiation and latent heat, this discrepancy might be a model shortcoming but it can be also generated by the lack of energy balance closure in the flux tower data (see Sect. 4.1). Compared with unCPLD and unCPLD-FT simulations, the overestimation was however reduced by the CPLD model simulations.

The correlation between observed and simulated surface heat fluxes with unCPLD, unCPLD-FT, and CPLD

275 model is shown in Fig. 4. Noticeably all the unCPLD/CPLD model scenarios, with different water and heat transfer physics, exhibit nearly identical statistical performance of surface fluxes simulations (Fig. 4). There is an overestimation of H reproduced by three model simulations. The CPLD model presented less overestimation of H compared to unCPLD models. The overall performance of the model in terms of turbulent flux simulations could be regarded as acceptable given current uncertainties in winter precipitation

280 and flux-tower observations in such a challenging environment, even though discrepancies exist during certain periods (Fig. 3).

3.2 Soil moisture simulations

The capability of the three models to reproduce the temporal dynamics of soil moisture is illustrated in Figure 5. By explicitly considering soil ice content, the unCPLD-FT and CPLD model capture well the response of

285 soil moisture dynamics to the freezing/thawing process. While the unCPLD model lacks such capability and maintains a higher soil moisture throughout the winter period, which then reflect in slightly lower water contents in the growing season. For all three models, the consistency between the measured and model simulated soil water content at five soil layers is satisfactory during the growing season, indicating the models' capability in portraying the effect of precipitation and root water uptake on the soil moisture conditions.

3.3 Soil temperature simulations

Five layers of soil temperature measurements were employed to test the performance of model in reproducing the soil thermal regime profiles (Fig. 6). During the growing period, all three models can well capture the dynamics of soil temperature at various depth with fluctuating atmospheric forcing. In this period, there is no significant difference among the three models with regards to the magnitude and temporal dynamics of soil temperature. During the freezing period, a general underestimation of soil temperature and overestimation of its diurnal fluctuations were found at shallower soil layers, which may indicate that there is some thermal buffering effect in reality not fully considered in the models. Compared with unCPLD-FT and CPLD models, the unCPLD model simulations have stronger diurnal fluctuations of soil temperature with an underestimation of temperature at the beginning of the freezing period and a considerable overestimation during the thawing phase. This results in an earlier date passing the 0°C threshold than in the unCPLD-FT simulations.

3.4 Soil ice content and water flux

The simulated time-series of soil ice content and water flux from both unCPLD and CPLD model simulations for soil layers below 2 cm are presented in Figure 7. As soil ice content measurements were not available, the freezing front propagation inferred from the soil temperature measurements was employed to qualitatively testify the model performance. A deeper presence of soil ice content was reproduced by the unCPLD-FT model, as indicated by a deeper freezing front propagation than the in-situ measurements. CPLD model presented a relative good match of soil freezing dynamics as it is physically constrained by the inter-dependence of liquid, ice, vapor, air components in soil pores. The phenomenon that a certain amount of liquid water flux moves upwards along with the freezing front can be clearly noticed from the unCPLD-FT and CPLD model simulations. As the soil matric potential changes sharply during the water phase change period, a certain amount of water fluxes will be forced towards the phase changing region, a phenomenon known as cryosuction. Such a phenomenon has already been demonstrated from theoretical and experimental perspectives by many researchers (Hansson et al., 2004; Watanabe et al., 2011; Yu et al., 2018). This is of course absent from the unCPLD model simulations (Fig. 7c). Nevertheless, the precipitation induced downward water flux can be observed in both models.

3.5 Simulations of land surface carbon fluxes

The eddy covariance derived and remote sensing (MODIS) observations of vegetation dynamics are compared with the model simulation in Fig. 8. When compared with in situ flux-tower observations, a slightly earlier growth and considerably earlier senescence of grassland with lower photosynthesis was inferred from MODIS *GPP* product (Fig. 8a). The mismatch in the phenology are likely a combined issue of 8-day (or longer if clouds are impeding the view) composite of MODIS products and challenge of translating vegetation reflectance signals into productivity or Leaf Area Index (LAI) during the grass senescent phase.

325   Trusting the temporal dynamics of flux-tower observations, the onset date of grassland appear to be well captured by both unCPLD and CPLD model simulations, while a delayed onset date is reproduced by unCPLD-FT model. Leaf senescence and dormancy phase are a bit delayed in the models when compared with flux-tower data and considerably delayed when compared to MODIS-LAI, even though the latter is particularly uncertain as described above. Although there is an observable underestimation of *GPP* compared to the eddy covariance measurements, the dynamics of *GPP*, which is mainly constrained by the

330   photosynthetic activity and environmental stresses, is reasonably reproduced by all model simulations.

The underestimation of GPP has magnified consequences in terms of reproducing *NEE* dynamics by unCPLD/CPLD models. While this might be seen as a model shortcoming, there are a number of reasons that lead to question the reliability of the magnitude of carbon fluxes measurements at this site. By checking other ecosystem productivity under similar conditions, the annual average *GPP* for the Tibetan plateau meadow

335   ecosystem ranges from 300 to 935 g C m^{-2} yr^{-1}, while annual average *NEE* ranges from -79 to -213 g C m^{-2} yr^{-1} (see the literature summary in the Supplement Table S2). While the EC system used in this experimental site observes an annual *GPP* and *NEE* as 1132.52 and -293.24 g C m^{-2} yr^{-1}. Both the *GPP* and *NEE* measured fluxes are significantly larger than previous estimates of carbon exchange for such a type of ecosystem (and representative of much more productive ecosystems) and are unlikely to be correct in magnitude. The

340   ecosystem respiration (R_{eco}), indicating the respiration of activity of all living organisms in an ecosystem is shown in Fig. 8d. The performance of all three model simulations in reproducing R_{eco} dynamics can be characterized as an overall good match with regards to the magnitude and seasonal dynamics of R_{eco}, which further suggest the discrepancy in observed/simulated *GPP* is the driver of the discrepancy of *NEE*.

The difference in the soil liquid water/temperature profile simulations between the CPLD and unCPLD

345   models (as shown in Fig. 5 & 6) resulted in difference in simulated vegetation dynamics, especially concerning the leaf onset date, which is affected by integrated winter soil temperatures. The unCPLD simulations have a slightly lower vegetation activity compared to the CPLD model simulations either because of a delayed leaf onset (unCPLD-FT) or because of a slightly enhanced water-stress (unCPLD) induced by the different soil-moisture dynamics during the winter season. Indeed, there is a slight lower root zone

350   moisture produced by the unCPLD model (Fig. 5), which affects the plant photosynthesis and growth, thus the vegetation dynamics in T&C. The unCPLD-FT model has a delay in the vegetation onset date, due to its prolonged freezing conditions as derived from soil temperature simulations than the other simulations.

4 Discussion

4.1 Surface energy balance closure

355   The energy balance closure problem, usually identified because the sum of latent (*LE*) and sensible (*H*) heat fluxes is less than the available energy (*Rn-G$_0$*), is quite common in eddy covariance measurements (Leuning et al., 2012;Wilson et al., 2002). The energy imbalance of EC measurements is particularly significant at the sites over the Tibetan Plateau (Tanaka et al., 2003;Yang et al., 2004;Zheng et al., 2014). Figure 9 presents

the energy balance imbalance of hourly *LE* and *H* by the eddy covariance measurements, observed *Rn* by the

360   four-component radiation measurements, and the estimated ground heat flux (G_0) by CPLD model. The sum of measured *LE* and *H* was significantly less than *Rn*, with the slope of 0.59 (Fig. 9a). Usually, the measurements of radiation are reliable (Yang et al., 2004). If we assume that the turbulence fluxes (*LE*, *H*) measurements were accurate, then the rest of energy (around 41% of *Rn*) should be theoretically consumed by ground heat flux G_0, which is clearly impossible. When compared to the available energy (*Rn-G_0*), the

365   slope was increased to 0.70 (Fig. 9b). Table 1 further demonstrated that the energy imbalance problem was significant across all seasons. The seasonal variation of energy closure ratio (ECR) can be identified for the case *LE+H versus Rn-G_0*, similar to the research of Tanaka et al. (2003), i.e., a good energy closure during the pre-monsoon periods while a degraded one during the summer monsoon periods.

These problems are clearly suggesting that care should be taken in the model to data comparison, but they

370   are not affecting the comparison among models with different complexity as we did not force any parameter calibration or data-fitting procedure, but simply rely on physical constraints, literature, and expert knowledge to assign model parameters.

4.2 Effects on water budget components

The effect of different model scenarios on soil water budget components is illustrated in Fig. 10. T&C model

375   can describe in details the different water budget components. Precipitation can be partitioned into vegetation interception, surface runoff, and infiltration. Infiltrated water can then be used for surface evaporation (*Es*), root water extraction (transpiration, *Tv*), and changes in soil water storage (ΔVs). The other evaporation components, i.e., evaporation from intercepted canopy water (E_{IN}) and snow cover (E_{SN}), can be further distinguished by T&C model. A certain amount of water will drain below the bottom of the 3 m soil column

380   as deep leakage (L_K).

All model cases demonstrated that most of the precipitation is used by ET. Compared to the unCPLD case, less water was consumed by ET according to unCPLD-FT simulations. This is due to the less vegetation transpiration (*Tv*) and intercepted canopy water evaporation (E_{IN}) amount because of cooler late winter temperatures and the late beginning of the active vegetation season. This explains the higher value of ΔVs

385   for unCPLD-FT simulation (5.22%) than that of unCPLD simulation (2.88%). With explicit consideration of soil ice, hydraulic conductivity is reduced and vertical water flow is retarded during the frozen period. However, at the end of the freezing period, the unCPLD-FT simulation presents a delayed vegetation onset thus a decrease of ecosystem water consumption, which favors percolation toward deeper layers and the bottom leakage. Such a positive effect on the bottom leakage flux was slightly weaker than the negative effect

390   (impeded water flow) due to frozen soil throughout the winter season. These results indicate that the presence of seasonal frozen soil can mediate the water storage in vadose zone via both hydrological and plant physiological controls.

The effect of coupled water and heat physics (unCPLD v.s. CPLD model) on the water budget components can be summarized as: i) the amount of ecosystem water consumption ET was reduced, due to the damped

395   surface evaporation process (evaporation from soil surface and intercepted water). ii) water storage amount in the vadose zone increased while the bottom leakage decreased. We attribute this to the way ice content is simulated in the CPLD simulation, and also to the temperature dependence of soil hydraulic conductivity. Taking into account the fully coupled water and heat physics modify the temporal dynamics of ice formation and thawing in the soil and activates temperature effects on water flow (i.e., low soil temperature will slow

400   down water movement). That implies that soil water flow toward and at the bottom soil layer is retarded when coupled water and heat physics is considered (as reflected by less leakage water flux for CPLD simulations).

4.3 The potential influential pathways of different mass/heat transfer processes

Given the same atmospheric forcing and the same model structure to represent land-surface exchanges and

405   vegetation dynamics, how water/heat transfer processes are represented in the soil generates differences in SM and ST vertical profiles. From the perspective of energy and carbon fluxes, the convective heat flux and explicit frozen soil physics are taken into account in the CPLD model while they are not considered in the unCPLD models. The liquid water flux induced convective heat flux is mostly relevant during the frozen period. As it has been observed, a certain amount of liquid water/vapor flux moving toward the freezing front

410   (Fig. 7), resulting in a convective heat toward the front. Such amount of heat and mostly the heat release by freezing and consumed by the melting processes slows down the freezing/thawing process and decreases the diurnal and seasonal temperature fluctuations (Fig. 5). Different soil thermal profiles have consequences on the vegetation dynamic process (Fig. 9), mainly by modifying the temperature profile in the soil, which affects the beginning of the growing season and the subsequent simulated photosynthesis and growth

415   processes. From the perspective of water fluxes, it is during the frozen period that water and heat transfer process are tightly coupled. Both the explicit consideration of soil ice and coupled water and heat physics can affect the vadose zone water flow via altering the hydraulic conductivity. This is testified by the fact that even the unCPLD-FT simulation accounting for soil-freezing in a simplified way in comparison to STEMMUS (e.g., the CPLD simulation) cannot recover the exact same dynamics of ice content (Fig. 7),

420   which impacts leaf onset and to a less extent hydrological fluxes. However, in the rest of the year the simplified solution of vadose zone physics of T&C leads to very similar results as the coupled one, suggesting that most of the additional physics does not modify substantially the ecohydrological response.

5 Conclusion

The detailed vadose zone process model STEMMUS and the ecohydrological model T&C were coupled to

425   investigate the effect of various model complexities in simulating water and energy transfer and seasonal ecohydrological dynamics over a typical Tibetan meadow. The results indicate that the original T&C model tended to overestimate the variability and magnitude of soil temperature during the freezing period and the freezing-thawing transition period. Such mismatches were ameliorated by the inclusion of soil ice content and freezing-thawing to the original model and further improved by the model with explicit consideration of

430   soil ice content dynamics and coupled water and heat physics. For the largest part of the simulated period, we found that a simplified treatment of vadose zone dynamics is sufficient to reproduce satisfactory energy, water and carbon fluxes – given uncertainty in the flux-tower observations. Additional complexity in vadose zone representation is mostly significant during the freezing and thawing periods as ice content simulations differs among models and a certain amount of water moving towards the freezing front was mostly

435   reproduced by the coupled model while it cannot be simulated by the original model and the modified model cannot account for the heat associated with this water movement. These differences have an impact (even though limited to the beginning of the growing season) on vegetation dynamics. The leaf onset is better captured by the unCPLD and CPLD models, while a delayed onset date was reproduced by unCPLD-FT model. Nonetheless, overall patterns for the rest of the year do not differ considerably among simulations,

440   which suggest that vadose zone dynamics with a fully coupled water-heat model treatment are not different enough to affect the overall ecosystem response. This suggests that the additional complexity might be more needed for specific vadose zone studies and investigation of permafrost thawing rather than for ecohydrological applications. In summary, our investigations using different models of vadose zone physics could be helpful to guide the development of future earth system model applications as they suggest that a

445   certain degree of complexity might be necessary only in specific analyses.

Data availability. The soil hydraulic/thermal property data can be accessed from 4TU. Center for Research Data (https://doi.org/10.4121/uuid:61db65b1-b2aa-4ada-b41e-61ef70e57e4a). The other relevant data are

450   available from https://doi.org/10.6084/m9.figshare.12058038.v1 or from Data Archiving and Networked Services (DANS) https://easy.dans.knaw.nl/ui/datasets/id/easy-dataset:160877 upon registration.

Author contribution. Conceptualization, Z.S. and Y.Z.; methodology, L.Y., Y.Z., and S.F.; writing - original draft preparation, L.Y., Y.Z., S.F., Z.S.; writing – review & editing, L.Y.,Y.Z., S.F., Z.S.

455

Competing interests. The authors declare that they have no conflict of interest.

Acknowledgment

This work is supported by the National Natural Science Foundation of China (grant no. 41971033) and supported by the Fundamental Research Funds for the Central Universities, CHD (grant no. 300102298307).

460   The authors would like to thank the editor and referees for their constructive comments and suggestions on improving the manuscript.

References

Bittelli, M., Ventura, F., Campbell, G. S., Snyder, R. L., Gallegati, F., and Pisa, P. R.: Coupling of heat, water vapor, and liquid water fluxes to compute evaporation in bare soils, J. Hydrol., 362, 191-205, https://doi.org/10.1016/j.jhydrol.2008.08.014, 2008.

Cheng, G., and Wu, T.: Responses of permafrost to climate change and their environmental significance, Qinghai-Tibet Plateau, Journal of Geophysical Research: Earth Surface, 112, 10.1029/2006JF000631, 2007.

Clark, M. P., Nijssen, B., Lundquist, J. D., Kavetski, D., Rupp, D. E., Woods, R. A., Freer, J. E., Gutmann, E. D., Wood, A. W., Brekke, L. D., Arnold, J. R., Gochis, D. J., and Rasmussen, R. M.: A unified approach for process-based hydrologic modeling: 1. Modeling concept, Water Resour. Res., 51, 2498-2514, 10.1002/2015wr017198, 2015.

Dall'Amico, M., Endrizzi, S., Gruber, S., and Rigon, R.: A robust and energy-conserving model of freezing variably-saturated soil, Cryosphere, 5, 469-484, 10.5194/tc-5-469-2011, 2011.

Dente, L., Vekerdy, Z., Wen, J., and Su, Z.: Maqu network for validation of satellite-derived soil moisture products, Int. J. Appl. Earth Obs. Geoinf., 17, 55-65, 10.1016/j.jag.2011.11.004, 2012.

Edlefsen, N., and Anderson, A.: Thermodynamics of soil moisture, Hilgardia, 15, 31-298, 1943.

Farouki, O. T.: The thermal properties of soils in cold regions, Cold Regions Sci. Tech., 5, 67-75, 10.1016/0165-232X(81)90041-0, 1981.

Fatichi, S., Ivanov, V. Y., and Caporali, E.: A mechanistic ecohydrological model to investigate complex interactions in cold and warm water-controlled environments: 1. Theoretical framework and plot-scale analysis, Journal of Advances in Modeling Earth Systems, 4, 10.1029/2011ms000086, 2012a.

Fatichi, S., Ivanov, V. Y., and Caporali, E.: A mechanistic ecohydrological model to investigate complex interactions in cold and warm water-controlled environments: 2. Spatiotemporal analyses, Journal of Advances in Modeling Earth Systems, 4, 10.1029/2011ms000087, 2012b.

Fatichi, S., and Ivanov, V. Y.: Interannual variability of evapotranspiration and vegetation productivity, Water Resour. Res., 50, 3275-3294, 10.1002/2013wr015044, 2014.

Fatichi, S., Leuzinger, S., Paschalis, A., Langley, J. A., Donnellan Barraclough, A., and Hovenden, M. J.: Partitioning direct and indirect effects reveals the response of water-limited ecosystems to elevated

490   CO_2, Proceedings of the National Academy of Sciences, 113, 12757-12762, 10.1073/pnas.1605036113, 2016a.

Fatichi, S., Pappas, C., and Ivanov, V. Y.: Modeling plant–water interactions: an ecohydrological overview from the cell to the global scale, WIREs Water, 3, 327-368, 10.1002/wat2.1125, 2016b.

Fatichi, S., and Pappas, C.: Constrained variability of modeled T:ET ratio across biomes, Geophys. Res. Lett., 44, 6795-6803, 10.1002/2017gl074041, 2017.

495   Fuchs, M., Campbell, G. S., and Papendick, R. I.: An Analysis of Sensible and Latent Heat Flow in a Partially Frozen Unsaturated Soil, Soil Sci. Soc. Am. J., 42, 379-385, 10.2136/sssaj1978.03615995004200030001x, 1978.

Gouttevin, I., Krinner, G., Ciais, P., Polcher, J., and Legout, C.: Multi-scale validation of a new soil freezing scheme for a land-surface model with physically-based hydrology, The Cryosphere, 6, 407-430, 10.5194/tc-

500   6-407-2012, 2012.

Hansson, K., Šimůnek, J., Mizoguchi, M., Lundin, L. C., and van Genuchten, M. T.: Water flow and heat transport in frozen soil: Numerical solution and freeze-thaw applications, Vadose Zone J., 3, 693-704, 2004.

Hao, Y. B., Cui, X. Y., Wang, Y. F., Mei, X. R., Kang, X. M., Wu, N., Luo, P., and Zhu, D.: Predominance of Precipitation and Temperature Controls on Ecosystem CO2 Exchange in Zoige Alpine Wetlands of

505   Southwest China, Wetlands, 31, 413-422, 10.1007/s13157-011-0151-1, 2011.

He, H., Liu, M., Xiao, X., Ren, X., Zhang, L., Sun, X., Yang, Y., Li, Y., Zhao, L., Shi, P., Du, M., Ma, Y., Ma, M., Zhang, Y., and Yu, G.: Large-scale estimation and uncertainty analysis of gross primary production in Tibetan alpine grasslands, Journal of Geophysical Research: Biogeosciences, 119, 466-486, 10.1002/2013jg002449, 2014.

510   Johansen, O.: Thermal conductivity of soils, PhD, University of Trondheim, 236 pp., 1975.

Lasslop, G., Reichstein, M., Papale, D., Richardson, A. D., Arneth, A., Barr, A., Stoy, P., and Wohlfahrt, G.: Separation of net ecosystem exchange into assimilation and respiration using a light response curve approach: critical issues and global evaluation, Global Change Biology, 16, 187-208, 2010.

Lawrence, D., Fisher, R., Koven, C., Oleson, K., Swenson, S., and Vertenstein, M.: Technical description of

515   version 5.0 of the Community Land Model (CLM), available at: http://www.cesm.ucar.edu/models/cesm2/land/CLM50_Tech_Note.pdf, 2018.

Lawrence, D. M., Fisher, R. A., Koven, C. D., Oleson, K. W., Swenson, S. C., Bonan, G., Collier, N., Ghimire, B., van Kampenhout, L., Kennedy, D., Kluzek, E., Lawrence, P. J., Li, F., Li, H., Lombardozzi, D., Riley, W. J., Sacks, W. J., Shi, M., Vertenstein, M., Wieder, W. R., Xu, C., Ali, A. A., Badger, A. M., Bisht,

520   G., van den Broeke, M., Brunke, M. A., Burns, S. P., Buzan, J., Clark, M., Craig, A., Dahlin, K., Drewniak, B., Fisher, J. B., Flanner, M., Fox, A. M., Gentine, P., Hoffman, F., Keppel-Aleks, G., Knox, R., Kumar, S., Lenaerts, J., Leung, L. R., Lipscomb, W. H., Lu, Y., Pandey, A., Pelletier, J. D., Perket, J., Randerson, J. T., Ricciuto, D. M., Sanderson, B. M., Slater, A., Subin, Z. M., Tang, J., Thomas, R. Q., Val Martin, M., and Zeng, X.: The Community Land Model Version 5: Description of New Features, Benchmarking, and Impact

525   of Forcing Uncertainty, Journal of Advances in Modeling Earth Systems, 11, 4245-4287, 10.1029/2018ms001583, 2019.

Lee, H. S., Matthews, C. J., Braddock, R. D., Sander, G. C., and Gandola, F.: A MATLAB method of lines template for transport equations, Environ. Model. Software, 19, 603-614, https://doi.org/10.1016/j.envsoft.2003.08.017, 2004.

530   Leuning, R., van Gorsel, E., Massman, W. J., and Isaac, P. R.: Reflections on the surface energy imbalance problem, Agr. Forest Meteorol., 156, 65-74, https://doi.org/10.1016/j.agrformet.2011.12.002, 2012.

Liu, X., and Chen, B.: Climatic warming in the Tibetan Plateau during recent decades, Int. J. Climatol., 20, 1729-1742, 10.1002/1097-0088(20001130)20:14<1729::AID-JOC556>3.0.CO;2-Y, 2000.

Mastrotheodoros, T., Pappas, C., Molnar, P., Burlando, P., Keenan, T. F., Gentine, P., Gough, C. M., and

535   Fatichi, S.: Linking plant functional trait plasticity and the large increase in forest water use efficiency, Journal of Geophysical Research: Biogeosciences, 122, 2393-2408, 10.1002/2017jg003890, 2017.

Milly, P. C. D.: Moisture and heat transport in hysteretic, inhomogeneous porous media: A matric head-based formulation and a numerical model, Water Resour. Res., 18, 489-498, 10.1029/WR018i003p00489, 1982.

Mwangi, S., Zeng, Y., Montzka, C., Yu, L., and Su, Z.: Assimilation of Cosmic-Ray Neutron Counts for the

540   Estimation of Soil Ice Content on the Eastern Tibetan Plateau, Journal of Geophysical Research: Atmospheres, 125, e2019JD031529, 10.1029/2019jd031529, 2020.

Myneni, R., Knyazikhin, Y., and Park, T.: MCD15A3H MODIS/Terra+Aqua Leaf Area Index/FPAR 4-Day L4 Global 500m SIN Grid V006, NASA EOSDIS Land Processes DAAC, 2015.

Niu, B., He, Y., Zhang, X., Fu, G., Shi, P., Du, M., Zhang, Y., and Zong, N.: Tower-Based Validation and

545   Improvement of MODIS Gross Primary Production in an Alpine Swamp Meadow on the Tibetan Plateau, Remote Sensing, 8, 592, 2016.

Niu, G.-Y., Yang, Z.-L., Mitchell, K. E., Chen, F., Ek, M. B., Barlage, M., Kumar, A., Manning, K., Niyogi, D., Rosero, E., Tewari, M., and Xia, Y.: The community Noah land surface model with multiparameterization options (Noah-MP): 1. Model description and evaluation with local-scale measurements, Journal of

550   Geophysical Research: Atmospheres, 116, 10.1029/2010jd015139, 2011.

Papale, D., Reichstein, M., Aubinet, M., Canfora, E., Bernhofer, C., Kutsch, W., Longdoz, B., Rambal, S., Valentini, R., Vesala, T., and Yakir, D.: Towards a standardized processing of Net Ecosystem Exchange measured with eddy covariance technique: algorithms and uncertainty estimation, Biogeosciences, 3, 571-583, 10.5194/bg-3-571-2006, 2006.

555   Pappas, C., Fatichi, S., and Burlando, P.: Modeling terrestrial carbon and water dynamics across climatic gradients: does plant trait diversity matter?, New Phytologist, 209, 137-151, 10.1111/nph.13590, 2016.

Qin, Y., Lei, H., Yang, D., Gao, B., Wang, Y., Cong, Z., and Fan, W.: Long-term change in the depth of seasonally frozen ground and its ecohydrological impacts in the Qilian Mountains, northeastern Tibetan Plateau, J. Hydrol., 542, 204-221, https://doi.org/10.1016/j.jhydrol.2016.09.008, 2016.

560   Reichstein, M., Falge, E., Baldocchi, D., Papale, D., Aubinet, M., Berbigier, P., Bernhofer, C., Buchmann, N., Gilmanov, T., Granier, A., Grünwald, T., Havránková, K., Ilvesniemi, H., Janous, D., Knohl, A., Laurila,

T., Lohila, A., Loustau, D., Matteucci, G., Meyers, T., Miglietta, F., Ourcival, J.-M., Pumpanen, J., Rambal, S., Rotenberg, E., Sanz, M., Tenhunen, J., Seufert, G., Vaccari, F., Vesala, T., Yakir, D., and Valentini, R.: On the separation of net ecosystem exchange into assimilation and ecosystem respiration: review and

565   improved algorithm, Global Change Biology, 11, 1424-1439, 10.1111/j.1365-2486.2005.001002.x, 2005.

Running Steve, Qiaozhen Mu, and Zhao, M.: MOD17A2H MODIS/Terra Gross Primary Productivity 8-Day L4 Global 500m SIN GridRep., NASA LP DAAC, 2015.

Scanlon, B. R., and Milly, P. C. D.: Water and heat fluxes in desert soils: 2. Numerical simulations, Water Resour. Res., 30, 721-733, 10.1029/93wr03252, 1994.

570   Su, Z., Wen, J., Dente, L., van der Velde, R., Wang, L., Ma, Y., Yang, K., and Hu, Z.: The Tibetan Plateau observatory of plateau scale soil moisture and soil temperature (Tibet-Obs) for quantifying uncertainties in coarse resolution satellite and model products, Hydrol. Earth Syst. Sci., 15, 2303-2316, 10.5194/hess-15-2303-2011, 2011.

Su, Z., de Rosnay, P., Wen, J., Wang, L., and Zeng, Y.: Evaluation of ECMWF's soil moisture analyses using

575   observations on the Tibetan Plateau, Journal of Geophysical Research: Atmospheres, 118, 5304-5318, 10.1002/jgrd.50468, 2013.

Tanaka, K., Tamagawa, I., Ishikawa, H., Ma, Y., and Hu, Z.: Surface energy budget and closure of the eastern Tibetan Plateau during the GAME-Tibet IOP 1998, J. Hydrol., 283, 169-183, https://doi.org/10.1016/S0022-1694(03)00243-9, 2003.

580   Tian, X., Yan, M., van der Tol, C., Li, Z., Su, Z., Chen, E., Li, X., Li, L., Wang, X., Pan, X., Gao, L., and Han, Z.: Modeling forest above-ground biomass dynamics using multi-source data and incorporated models: A   case   study   over   the   qilian   mountains,   Agr.   Forest   Meteorol.,   246,   1-14, https://doi.org/10.1016/j.agrformet.2017.05.026, 2017.

Wang, L., Liu, H., Sun, J., and Shao, Y.: Biophysical effects on the interannual variation in carbon dioxide

585   exchange of an alpine meadow on the Tibetan Plateau, Atmos. Chem. Phys., 17, 5119-5129, 10.5194/acp-17-5119-2017, 2017.

Wang, L., Liu, H., Shao, Y., Liu, Y., and Sun, J.: Water and CO2 fluxes over semiarid alpine steppe and humid alpine meadow ecosystems on the Tibetan Plateau, Theor. Appl. Climatol., 131, 547-556, 10.1007/s00704-016-1997-1, 2018.

590   Watanabe, K., Kito, T., Wake, T., and Sakai, M.: Freezing experiments on unsaturated sand, loam and silt loam, Ann. Glaciol., 52, 37-43, 10.3189/172756411797252220, 2011.

Wilson, K., Goldstein, A., Falge, E., Aubinet, M., Baldocchi, D., Berbigier, P., Bernhofer, C., Ceulemans, R., Dolman, H., Field, C., Grelle, A., Ibrom, A., Law, B. E., Kowalski, A., Meyers, T., Moncrieff, J., Monson,

R., Oechel, W., Tenhunen, J., Valentini, R., and Verma, S.: Energy balance closure at FLUXNET sites, Agr.
595   Forest Meteorol., 113, 223-243, https://doi.org/10.1016/S0168-1923(02)00109-0, 2002.

Wutzler, T., Lucas-Moffat, A., Migliavacca, M., Knauer, J., Sickel, K., Šigut, L., Menzer, O., and Reichstein,
M.: Basic and extensible post-processing of eddy covariance flux data with REddyProc, Biogeosciences, 15,
5015-5030, 10.5194/bg-15-5015-2018, 2018.

Yang, K., Koike, T., Ishikawa, H., and Ma, Y.: Analysis of the Surface Energy Budget at a Site of
600   GAME/Tibet using a Single-Source Model, Journal of the Meteorological Society of Japan. Ser. II, 82, 131-
153, 10.2151/jmsj.82.131, 2004.

Yu, L., Zeng, Y., Su, Z., Cai, H., and Zheng, Z.: The effect of different evapotranspiration methods on
portraying soil water dynamics and ET partitioning in a semi-arid environment in Northwest China, Hydrol.
Earth Syst. Sci., 20, 975-990, 10.5194/hess-20-975-2016, 2016a.

605   Yu, L., Zeng, Y., Wen, J., and Su, Z.: Liquid-Vapor-Air Flow in the Frozen Soil, Journal of Geophysical
Research: Atmospheres, 123, 7393-7415, 10.1029/2018jd028502, 2018.

Yu, M., Wang, G., and Chen, H.: Quantifying the impacts of land surface schemes and dynamic vegetation
on the model dependency of projected changes in surface energy and water budgets, Journal of Advances in
Modeling Earth Systems, 8, 370-386, 10.1002/2015ms000492, 2016b.

610   Zeng, Y., Su, Z., Wan, L., Yang, Z., Zhang, T., Tian, H., Shi, X., Wang, X., and Cao, W.: Diurnal pattern of
the drying front in desert and its application for determining the effective infiltration, Hydrol. Earth Syst.
Sci., 13, 703-714, 10.5194/hess-13-703-2009, 2009a.

Zeng, Y., Wan, L., Su, Z., Saito, H., Huang, K., and Wang, X.: Diurnal soil water dynamics in the shallow
vadose zone (field site of China University of Geosciences, China), Environ. Geol., 58, 11-23, 2009b.

615   Zeng, Y., Su, Z., Wan, L., and Wen, J.: A simulation analysis of the advective effect on evaporation using a
two-phase heat and mass flow model, Water Resour. Res., 47, W10529, 10.1029/2011WR010701, 2011a.

Zeng, Y., Su, Z., Wan, L., and Wen, J.: Numerical analysis of air-water-heat flow in unsaturated soil: Is it
necessary to consider airflow in land surface models?, Journal of Geophysical Research: Atmospheres, 116,
D20107, 10.1029/2011JD015835, 2011b.

620   Zeng, Y., Su, Z., van der Velde, R., Wang, L., Xu, K., Wang, X., and Wen, J.: Blending Satellite Observed,
Model Simulated, and in Situ Measured Soil Moisture over Tibetan Plateau, Remote Sensing, 8, 268, 2016.

Zeng, Y. J., and Su, Z. B.: STEMMUS : Simultaneous Transfer of Engery, Mass and Momentum in
Unsaturated Soil, ISBN: 978-90-6164-351-7, University of Twente, Faculty of Geo-Information and Earth
Observation (ITC), Enschede, 2013.

625   Zhang, G., Zhang, Y., Dong, J., and Xiao, X.: Green-up dates in the Tibetan Plateau have continuously
advanced from 1982 to 2011, Proceedings of the National Academy of Sciences, 110, 4309-4314,
10.1073/pnas.1210423110, 2013.

Zhao, H., Zeng, Y., Lv, S., and Su, Z.: Analysis of soil hydraulic and thermal properties for land surface
modeling over the Tibetan Plateau, Earth Syst. Sci. Data, 10, 1031-1061, 10.5194/essd-10-1031-2018, 2018.

630   Zhao, L., Li, J., Xu, S., Zhou, H., Li, Y., Gu, S., and Zhao, X.: Seasonal variations in carbon dioxide exchange in an alpine wetland meadow on the Qinghai-Tibetan Plateau, Biogeosciences, 7, 1207-1221, 10.5194/bg-7-1207-2010, 2010.

Zheng, D., Velde, R. v. d., Su, Z., Booij, M. J., Hoekstra, A. Y., and Wen, J.: Assessment of Roughness Length Schemes Implemented within the Noah Land Surface Model for High-Altitude Regions, J.
635   Hydrometeorol., 15, 921-937, 10.1175/jhm-d-13-0102.1, 2014.

Zheng, D., Van der Velde, R., Su, Z., Wang, X., Wen, J., Booij, M. J., Hoekstra, A. Y., and Chen, Y.: Augmentations to the Noah Model Physics for Application to the Yellow River Source Area. Part I: Soil Water Flow, J. Hydrometeorol., 16, 2659-2676, 10.1175/JHM-D-14-0198.1, 2015a.

Zheng, D., Van der Velde, R., Su, Z., Wen, J., Booij, M. J., Hoekstra, A. Y., and Wang, X.: Under-canopy
640   turbulence and root water uptake of a Tibetan meadow ecosystem modeled by Noah-MP, Water Resour. Res., 51, 5735-5755, 10.1002/2015wr017115, 2015b.

Zhuang, R., Zeng, Y., Manfreda, S., and Su, Z.: Quantifying Long-Term Land Surface and Root Zone Soil Moisture over Tibetan Plateau, Remote Sensing, 12, 509, 2020.

Tables and Figures

645

Table 1. Monthly values of energy closure ratio derived from eddy covariance measured LE + H versus Rn and Rn-G_0, respectively (Dec. 2017-Aug. 2018). G_0, the ground heat flux, was estimated by CPLD model.

Energy closure ratio	Dec	Jan	Feb	Mar	Apr	May	Jun	Jul	Aug
($LE+H$) vs Rn	0.58	0.58	0.61	0.45	0.53	0.55	0.55	0.57	0.59
($LE+H$) vs (Rn-G_0)	0.98	0.90	0.90	0.51	0.62	0.68	0.64	0.63	0.67
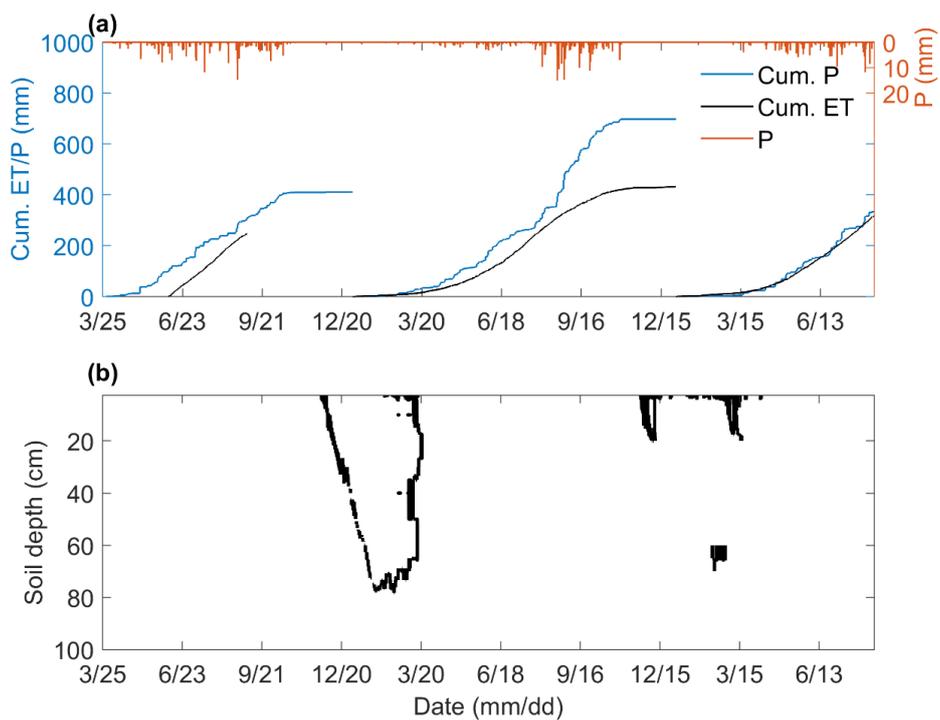
650

Figure 1. Observed cumulative precipitation and evapotranspiration (a) and observed propagation of freezing/thawing front (b) for the period 25 Mar. 2016- 12 Aug. 2018 at Maqu site.
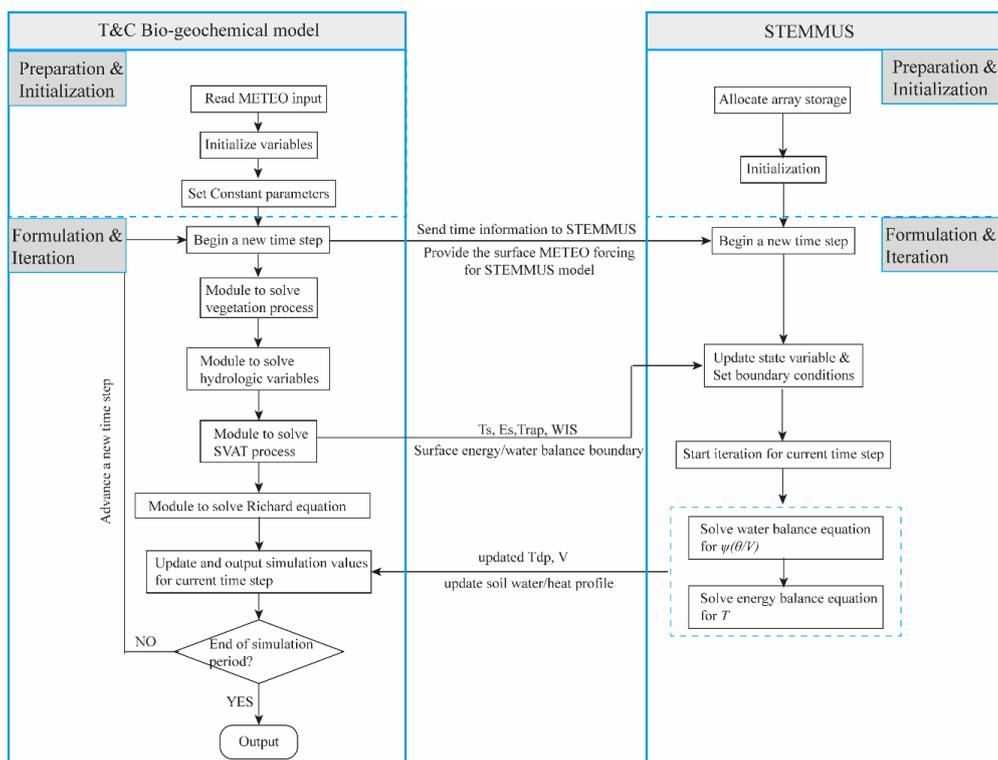
Figure 2. Coupling procedure of STEMMUS and T&C model. METEO is the meteorology forcing, SVAT is acronym for the Soil-Vegetation-Atmosphere mass and heat Transfer. Ts, Es, Trap, WIS are the surface temperature, soil evaporation, plant transpiration, and incoming water flux to the soil, respectively. T_{dp}, V are the soil profile information of temperature in °C and water volume in mm.

660
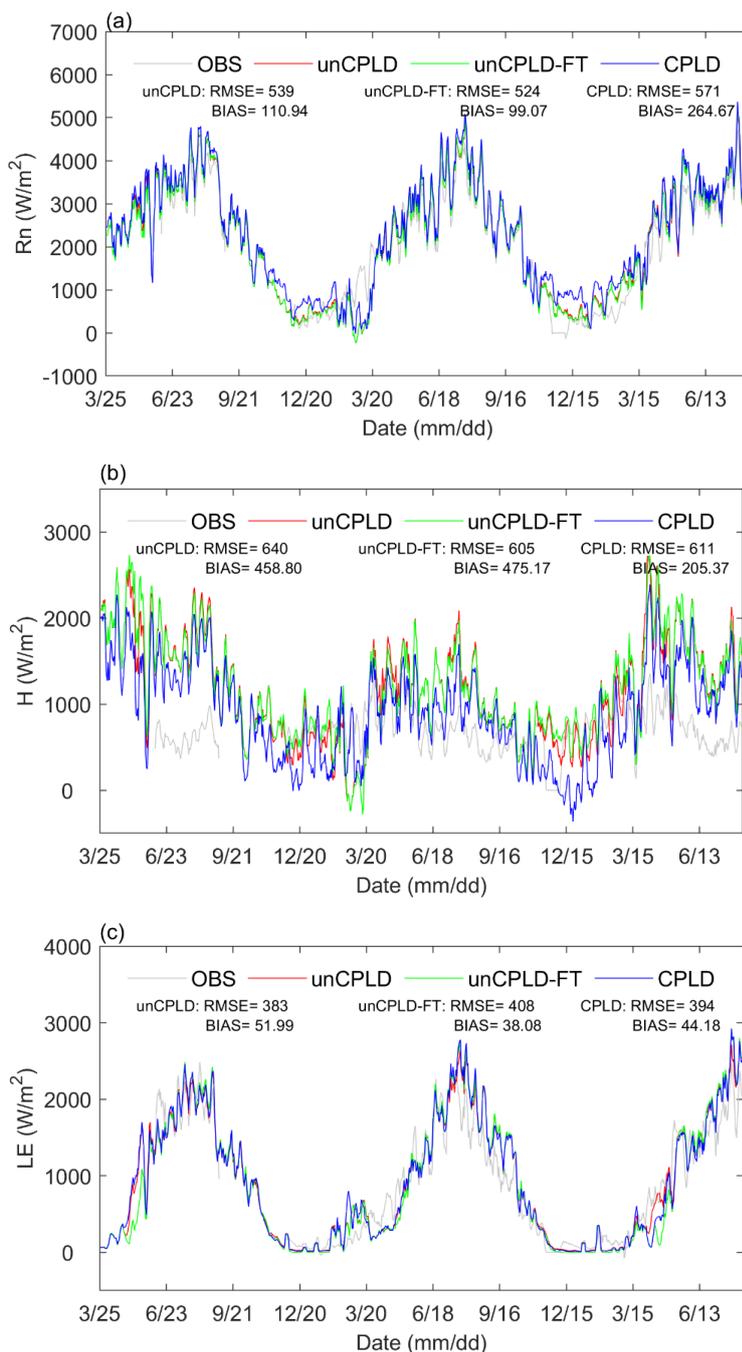
Figure 3. Comparison of observed and simulated 5-day moving average dynamics of net radiation(Rn), latent heat flux(LE), and sensible heat flux(H) using the original (uncoupled) T&C (unCPLD) , T&C with consideration of FT process (unCPLD-FT) and coupled T&C and STEMMUS (CPLD) model.

665
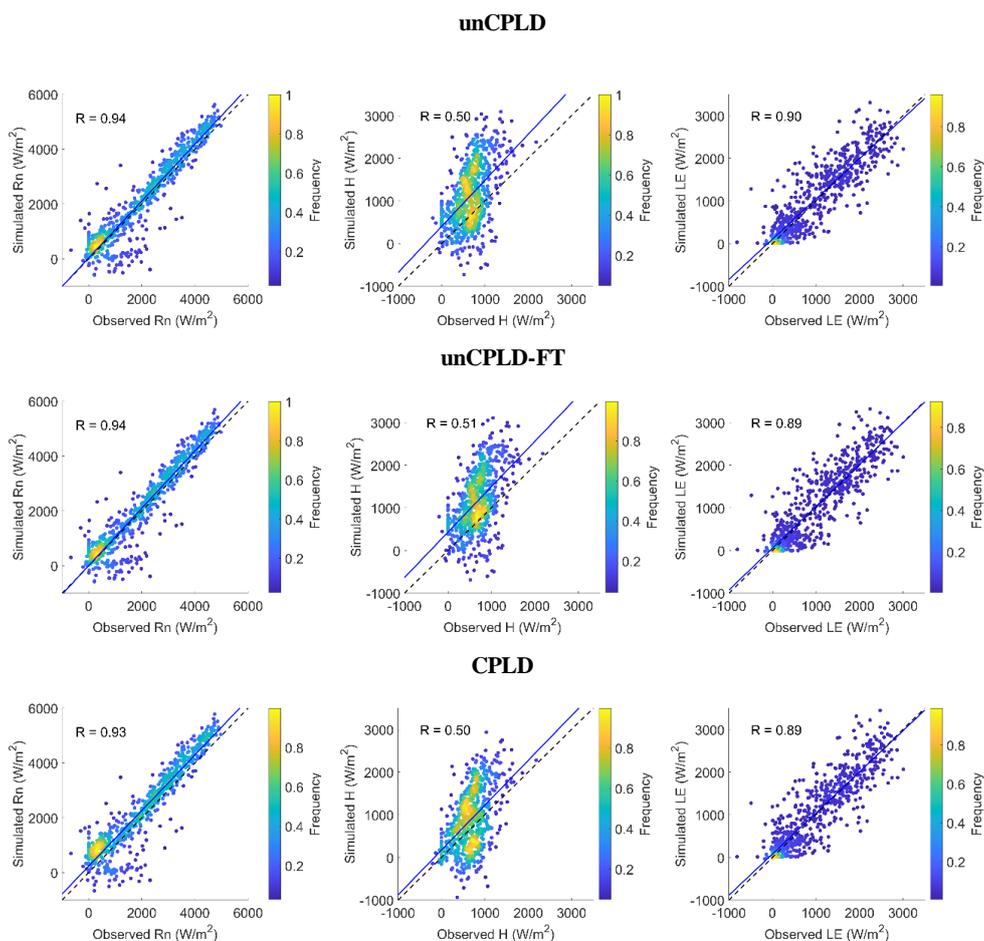
Figure 4. Scatter plots of observed and model simulated daily surface fluxes (net radiation: Rn, latent heat: LE and sensible heat flux: H) using the original (uncoupled) T&C (unCPLD), T&C with consideration of FT process (unCPLD-FT) and coupled T&C and STEMMUS (CPLD) model, with the color indicating the occurrence frequency of surface flux values.

670
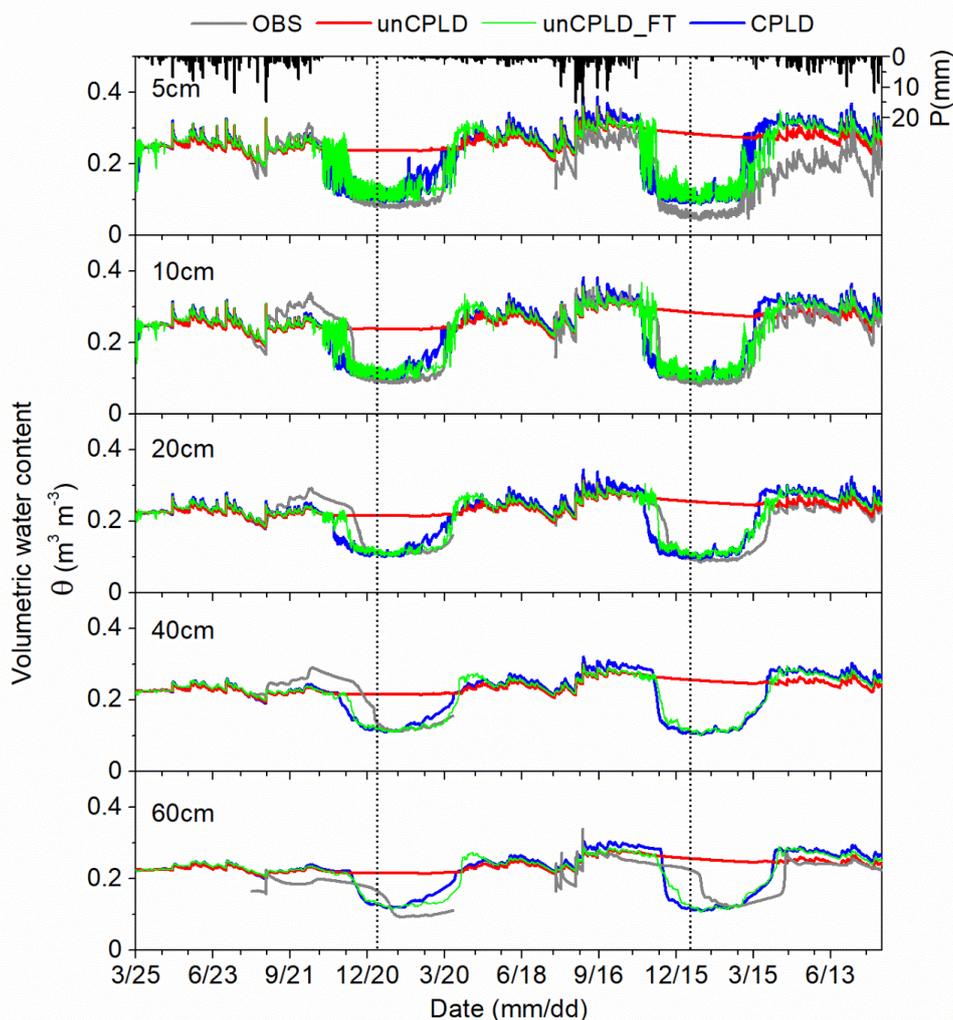
Figure 5. Measured and estimated soil moisture at various soil layers using uncoupled T&C (unCPLD), uncoupled T&C with FT process (unCPLD-FT) and coupled T&C and STEMMUS (CPLD) model. Note that in unCPLD model, soil ice content is not explicitly considered, thus all the water remains in a liquid phase, which is leading to a strong overestimation of winter soil water content in frozen soils.

675

680
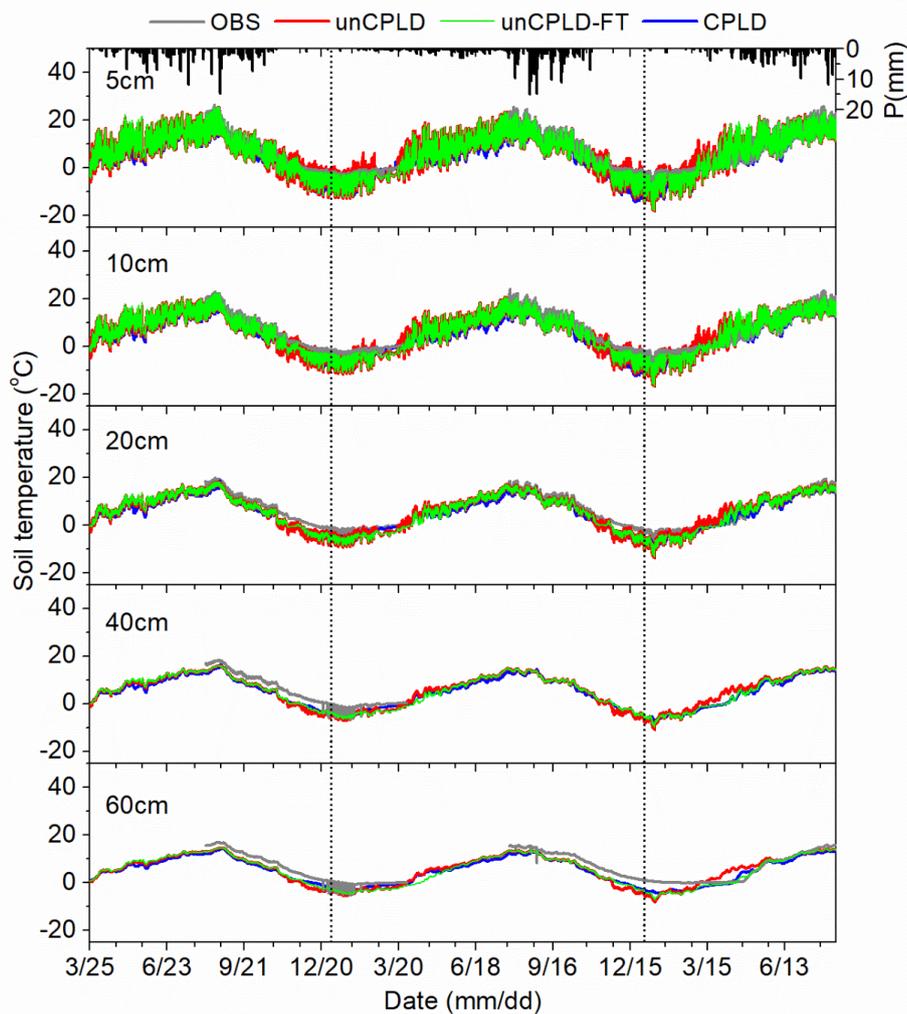
Figure 6. Measured and simulated soil temperature at various soil layers using uncoupled T&C (unCPLD), T&C with FT process (unCPLD-FT) and coupled T&C and STEMMUS (CPLD) model.

685
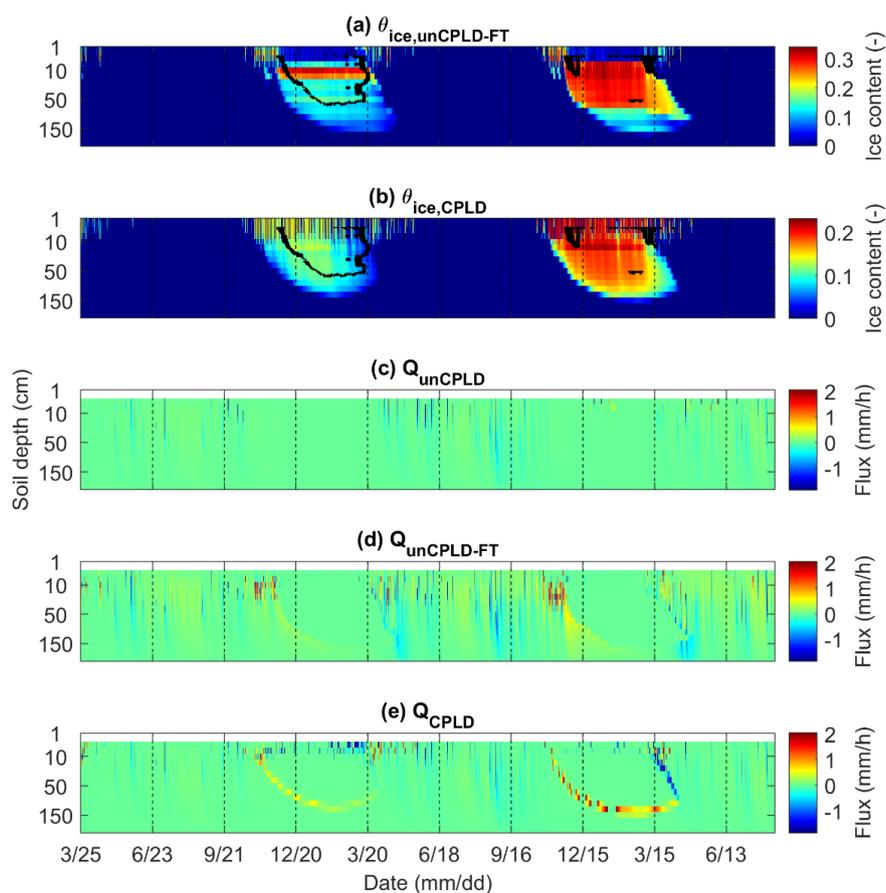
Figure 7. Soil ice content from (a) unCPLD-FT and (b) CPLD model simulations with freezing front propagation derived from the measured soil temperature and vertical water flux from (c) unCPLD, (d) unCPLD-FT and (e) CPLD model simulations, note that soil ice content was not presented for unCPLD model and the fluxes of top 1-2 cm soil layers were erased to highlight fluxes of the lower layers.

690

695
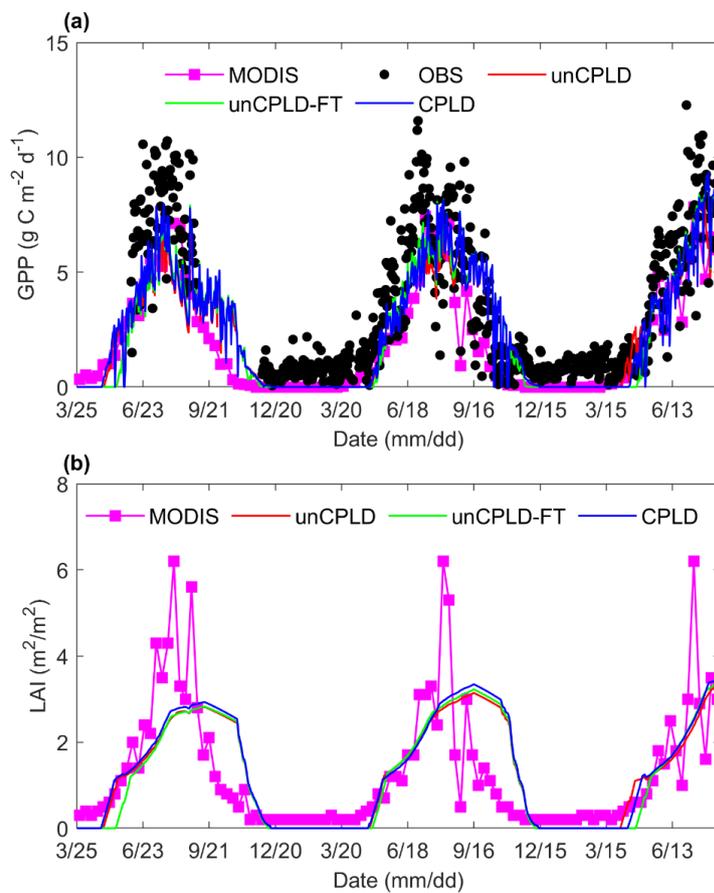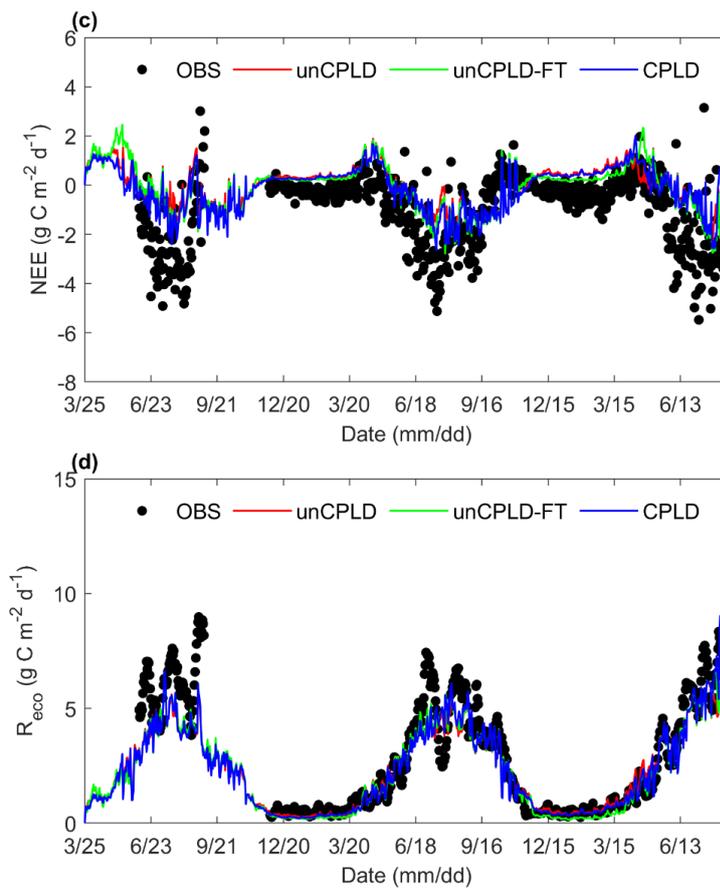
700

Figure 8. Comparison of observed flux-tower observations or MODIS remote sensing and simulated (a) GPP, (b) LAI, (c) NEE, and (d) R$_{eco}$ using unCPLD, unCPLD-FT, and CPLD model. MODIS refers to the data from MODIS-GPP and MODIS-LAI products.

705
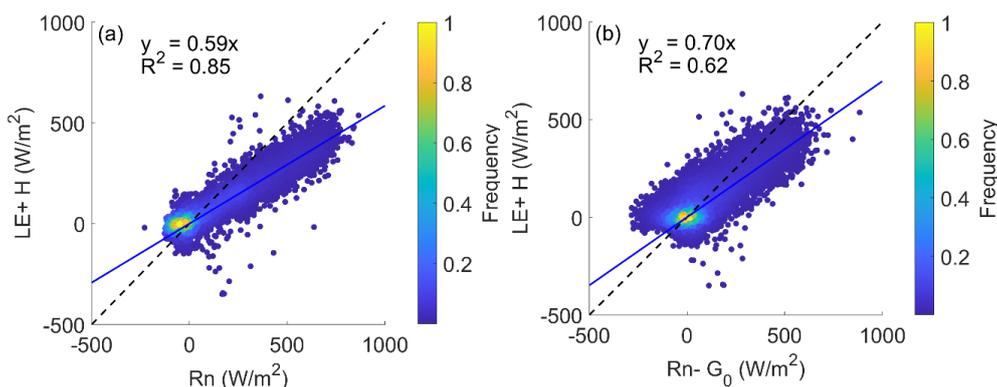
Figure 9. Scatter plots of eddy covariance measured LE + H versus (a) Rn and (b) Rn-G$_0$, with the color indicating the occurrence frequency of surface flux values. G$_0$, the ground heat flux, was estimated by CPLD model.

710
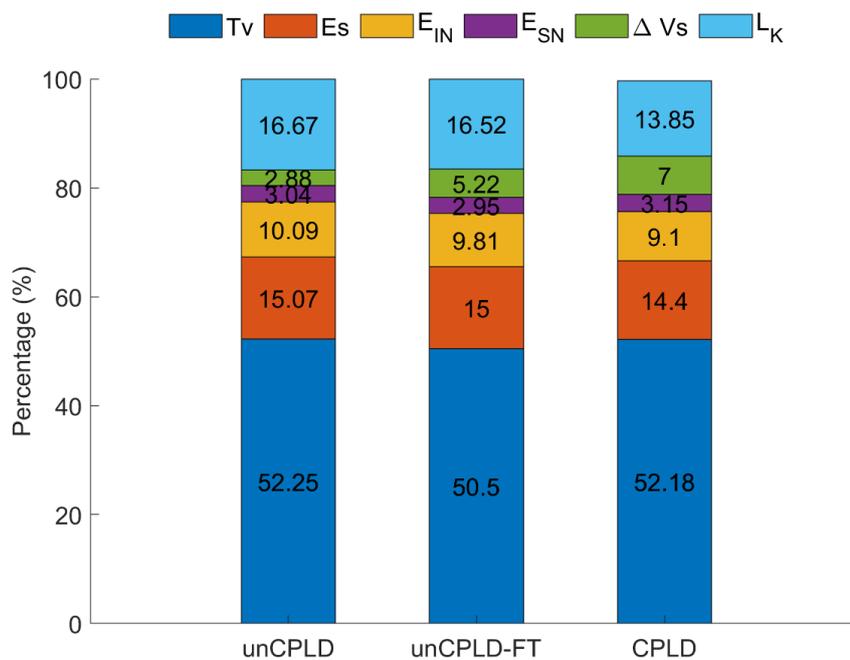
Figure 10. Comparison of the relative ratios of different water budget components to precipitation during the whole simulation period produced by different model scenarios.

715